Eur. Phys. J. B **61**, 457–463 (2008)
DOI: 10.1140/epjb/e2008-00100-7

THE EUROPEAN PHYSICAL JOURNAL B

Study on the spin-states of cobalt-based double-layer perovskite $Sr_2Y_{0.5}Ca_{0.5}Co_2O_7$

H. He[a] and W.Y. Zhang

National Laboratory of Solid State Microstructures and Department of Physics, Nanjing University, Nanjing 210093, P.R. China

Received 6 June 2007 / Received in final form 22 January 2008
Published online 7 March 2008 –

Abstract. The spin-states of cobalt based perovskite compounds depend sensitively on the valence state and local crystal environment of Co ions and the rich physical properties arise from strong coupling among charge, spin, and orbital degrees of freedom. While extensive studies have been carried out in the past, most of them concentrated on the isotropic compound $LaCoO_3$. In this paper, using the unrestricted Hartree-Fock approximation and the real-space recursion method, we have investigated the competition of various magnetically ordered spin-states of anisotropic double-layered perovskite $Sr_2Y_{0.5}Ca_{0.5}Co_2O_7$. The energy comparison among these states shows that the nearest-neighbor high-spin-intermediate-spin ferromagnetically ordered state is the relevant magnetic ground state of the compound. The magnetic structure and sizes of magnetic moments are consistent with the recent experimental observation.

PACS. 75.25.+z Spin arrangements in magnetically ordered materials – 71.20.-b Electron density of states and band structure of crystalline solids – 71.30.+h Metal-insulator transitions and other electronic transitions

1 Introduction

The spin-state transition is a common phenomenon in cobalt based perovskite compounds, the physical origin arises from close proximity between the Hund's coupling energy and crystal field splitting energy of Co-d orbitals. In the prototype compound $La_{1-x}Sr_xCoO_3$ [1–4], both photoemission spectra [5–8] and electrical resistivity measurements [9–12] suggested that there appears an insulator-metal transition at the doping concentration $x \sim 0.2$; moreover, this transition is often accompanied by a magnetic change from a nonmagnetic state to a ferromagnetically ordered state. To explore the nature of such spin-state transition in doped compounds, theoretical studies [13,14] have been done on the electronic structures of $La_{1-x}Sr_xCoO_3$ for the whole doping range $0.0 < x < 1.0$. It is found that the ground state changes from a low-spin state($t_{2g}^{6-x}e_g^0$) at low doping concentration $x < 0.25$ to a ferromagnetic intermediate-spin state($t_{2g}^5e_g^{1-x}$) at moderate doping $0.25 < x < 0.41$; for higher doping concentration $0.41 < x < 0.95$ the ground state of the system takes an intermediate-spin high-spin ($t_{2g}^5e_g^{1-x}$-$t_{2g}^4e_g^{2-x}$) ferromagnetically ordered state, which is followed by a high-spin state up to $x = 1.0$.

Such fascinating magnetic properties are not unique to the isotropic perovskite compound $La_{1-x}Sr_xCoO_3$, they also occur in layered perovskite compound $La_{2-x}Sr_xCoO_4$ [15,16]. The zero-field nuclear magnetic resonance investigation [15] suggested that the magnetic state of $La_{2-x}Sr_xCoO_4$ suddenly transforms from an antiferromagnetic state to a ferromagnetic state when doping concentration x is large ($x \geq 0.6$). The effective magnetic moment of $La_{2-x}Sr_xCoO_4$ [16] starts to decrease slowly at $x \sim 0.5$ and is followed by a sharp drop at $x \sim 0.7$, it becomes an almost constant $\sim 2.6\mu_B$ afterwards. At the same time, this process is also accompanied by a great reduction of electrical resistivity. These experimental observations lead Morimoto et al. [16] to conclude that a spin-state transition of Co^{+3} takes place from a high-spin state ($t_{2g}^4e_g^2$) to an intermediate-spin state ($t_{2g}^5e_g^1$) at $x \sim 0.7$.

Recently, the studies on the spin-state transition have been extended to other low dimensional Ruddlesden-Popper series [17,18]. Using the solid state reaction method under high pressure, Yamaura et al. [17] have successfully synthesized $n = 2$ member of the Ruddlesden-Popper series $Sr_2Y_{0.5}Ca_{0.5}Co_2O_7$. Polycrystalline samples of $Sr_2Y_{0.5}Ca_{0.5}Co_2O_7$ have been analyzed by the X-ray diffraction method and the crystal structures are found to belong to a space group of I4/mmm with the lattice parameters $a = b = 3.759$ Å and $c = 20.00$ Å. But the oxygen concentration is not accurately determined and this phase is also mixed with a small amount of $KClO_z$. The formal valence of Co ions is $Co^{+3.75}$, the magnetic measurements [17] showed that $Sr_2Y_{0.5}Ca_{0.5}Co_2O_7$ is a ferromagnet with Curie temperature $T_C = 169$ K, the

[a] e-mail: kelly_h2@hotmail.com

paramagnetic moment derived from the high temperature paramagnetic susceptibility is $2.89\mu_B$. The mixed high-spin low-spin ferromagnetic state is proposed based on the size of magnetic moments and valence states of purely ionic model. The transport property is strongly influenced by disorders, grain boundaries, and mixed phase of $KClO_z$, variable-hopping conductivity behavior is found instead of a metallic behavior.

While systematic studies have been done on the pseudo-cubic $LaCoO_3$ [1–14] and $La_{2-x}Sr_xCoO_4$ compounds [15,16], the investigation on other layer-structured cobalt based oxides of the Ruddlesden-Popper (RP) series structure is relatively new and few theoretical study exists. Thus, we have carried out the theoretical study in this paper on electronic and magnetic structures of $Sr_2Y_{0.5}Ca_{0.5}Co_2O_7$ compound [17]. As is well known, different spin-states can take place depending on the valence state of Co ions and local bond strength [1–14]. For Co^{3+} ions, high-spin(HS), intermediate-spin(IS), and low-spin(LS) states are the possibilities and their electronic configurations are $t_{2g}^4e_g^2(S=2)$, $t_{2g}^5e_g^1(S=1)$, and $t_{2g}^6e_g^0(S=0)$; while for Co^{4+} ions, the corresponding three spin-states are $t_{2g}^3e_g^2$(HS: $S=5/2$), $t_{2g}^4e_g^1$(IS: $S=3/2$), and $t_{2g}^5e_g^0$(LS: $S=1/2$). In $Sr_2Y_{0.5}Ca_{0.5}Co_2O_7$ compound [17], the formal valence of Co ions is 3.75, but the actual valence is close to 3 because of charge transfer between oxygen and cobalt caused by strong covalence bonding between the two [5]. To explore the most probable magnetic ground state, we have studied various possible metastable states with different Co spin-states and magnetic long range orders as a function of electrostatic crystal-field-splitting component. We find that the nearest neighbor HS-IS ferromagnetically ordered state is the most probable magnetic ground state of the system, the effective magnetic moment is also consistent with the experimentally measured one.

It should be mentioned that the recent discovery of superconductivity by Takada et al. [19] in the hydrated $Na_xCoO_2 \cdot yH_2O$ around $x \sim 0.3$ has generated a great interest in cobalt based oxides, this compound also belongs to a layer-structured type, but with hexagonal crystal symmetry. The fascinating electronic, magnetic, and superconducting properties of Na-doped CoO_2 have been extensively studied by both experimentalists and theoretists [19,21]. However, we shall restrict ourselves in this paper on the spin-state phenomenon in recently prepared $Sr_2Y_{0.5}Ca_{0.5}Co_2O_7$ compound [17].

The rest of this paper is organized as following. In Section 2, the well adopted multiband *d-p* Hamiltonian is briefly described in connection with transition metal oxides, the application of unrestricted Hartree-Fock approximation is outlined together with the real space recursion method for calculating the local Green's function. In Section 3, we analyze the relative stability of various magnetic states as a function of electrostatic crystal-field-splitting component and present the densities of states for those most relevant states. The conclusion is drawn in Section 4.

2 Theoretical model and formulation

The photoemission spectra measurement and *ab initio* band structure calculation [5,6] suggest that the dominant electronic states in the transition metal oxides near the Fermi energy are contributed by the transition metal *d*-orbitals and oxygen *p*-orbitals, the multiband *d-p* model Hamiltonian [22] contains all these essential orbitals in addition to the strong correlation among *d*-electrons described by on-site Coulomb and exchange interactions:

$$\begin{aligned} H = & \sum_{im\sigma} \varepsilon_{dm}^0 d_{im\sigma}^\dagger d_{im\sigma} + \sum_{jn\sigma} \varepsilon_p p_{jn\sigma}^\dagger p_{jn\sigma} \\ & + \sum_{ijmn\sigma} (t_{ij}^{mn} d_{im\sigma}^\dagger p_{jn\sigma} + h.c.) \\ & + \sum_{ijnn'\sigma} (t_{ij}^{nn'} p_{in\sigma}^\dagger p_{jn'\sigma} + h.c) + u \sum_{im} d_{im\uparrow}^\dagger d_{im\uparrow} d_{im\downarrow}^\dagger d_{im\downarrow} \\ & + \frac{1}{2}\tilde{u} \sum_{im\neq m'\sigma\sigma'} d_{im\sigma}^\dagger d_{im\sigma} d_{im'\sigma'}^\dagger d_{im'\sigma'} - J_H \\ & \times \sum_{im\neq m'} \mathbf{S}_{im} \cdot \mathbf{S}_{im'}. \end{aligned} \quad (1)$$

In equation (1), $d_{im\sigma}^\dagger$ ($d_{im\sigma}$) and $p_{jn\sigma}^\dagger$ ($p_{jn\sigma}$) denote the creation(annihilation) operators of an electron on Co *d*-orbital at site *i* and O *p*-orbital at site *j*, respectively. ε_{dm}^0 and ε_p are their corresponding on-site energies. *m* and *n* represent the orbital index and σ denotes the spin. The electrostatic part of crystal-field-splitting ($10Dq$) induced by local octahedron environment at Co ions is included in ε_{dm}^0, i.e., $\varepsilon_d^0(t_{2g}) = \varepsilon_d^0 - 4Dq$ and $\varepsilon_d^0(e_g) = \varepsilon_d^0 + 6Dq$ with ε_d^0 as the bare on-site energy of *d*-orbitals. The total crystal-field-splitting has, in addition to the electrostatic part, the contributions from on-site Coulomb repulsion, Hund's coupling as well as covalent bondings with neighboring O *p*-orbitals [23,24] which are taken into account through Hartree-Fock self-consistent band calculation. The cubic form of electrostatic crystal-field-splitting is a good approximation since neglected non-cubic contribution is on the order of 1%. t_{ij}^{mn} and $t_{ij}^{nn'}$ are the nearest neighbor hopping integrals for *p-d* and *p-p* orbitals, they are expressed in terms of Slater-Koster parameters ($pd\sigma$), ($pd\pi$), ($pp\sigma$), and ($pp\pi$) [25]. $\mathbf{S}_{im}$ is the spin operator of electron on Co-*d*'s *m*-orbital. $\tilde{u} = u - 5J_H/2$, the parameter u is related to the multiplet averaged *d-d* Coulomb interaction U via $u = U + (20/9)J_H$. The above Hamiltonian describes the itinerant nature of transition metal oxides. In localized electron picture with integer occupation numbers on orbitals Heisenberg-like Hamiltonian can be obtained by perturbation method where both double exchange and superexchange interactions are implicitly included, but the exchange interactions have a more complex form and depend on the specific electron occupations on various orbitals [26].

After linearizing the Hamiltonian equation (1) using the unrestricted Hartree-Fock approximation, the

following effective single particle Hamiltonian is obtained,

$$H = \sum_{im\sigma}\Big[\varepsilon^0_{dm} + un^d_{im\bar{\sigma}} - \frac{J_H}{2}\sigma(\mu^d_{it} - \mu^d_{im}) + \tilde{u}(n^d_{it} - n^d_{im})\Big]d^\dagger_{im\sigma}d_{im\sigma} + \sum_{jn\sigma}\varepsilon_p p^\dagger_{jn\sigma}p_{jn\sigma} + \sum_{ijmn\sigma}(t^{mn}_{ij}d^\dagger_{im\sigma}p_{jn\sigma} + h.c) + \sum_{ijnn'\sigma}(t^{nn'}_{ij}p^\dagger_{in\sigma}p_{jn'\sigma} + h.c.). \quad (2)$$

Here, $n^d_{im\sigma} = \langle d^\dagger_{im\sigma}d_{im\sigma}\rangle$ and $\mu^d_{im} = n^d_{im\uparrow} - n^d_{im\downarrow}$. n^d_{it} and μ^d_{it} are the total electron occupation and magnetic moment of Co d-orbitals. We have chosen the z-axis as spin quantization axis.

Using the real space recursion method, the above effective single particle Hamiltonian equation (2) can be mapped into a one-dimensional chain for a given starting orbital and the local Green's function for a given orbital can be easily calculated [27]

$$G^0_{m\sigma}(\omega) = \cfrac{b_0^2}{\omega - a_0 - \cfrac{b_1^2}{\omega - a_1 - \cfrac{b_2^2}{\omega - a_2 - \cfrac{b_3^2}{\omega - a_3 - \ldots}}}}. \quad (3)$$

a_i and b_i^2 are the recursion coefficients computed from the tridiagonalization of the tight-binding Hamiltonian matrix for a given starting orbital. The multiband terminator [28] is chosen to close the continuous fractional. To explore the possible magnetic ground state of $Sr_2Y_{0.5}Ca_{0.5}Co_2O_7$, we have considered various ordered magnetic states in an enlarged double cell of $Sr_2Y_{0.5}Ca_{0.5}Co_2O_7$, 33 levels are computed for each of the 124 independent orbitals. Our results have been checked for different levels to secure an energy accuracy better than 5 meV. The whole procedure is iterated self-consistently for a set of electron occupation numbers $n^d_{im\sigma}$. The density of states is obtained by $\rho_{ms}(\omega) = -(1/\pi)\mathrm{Im}G^0_{ms}(\omega)$, which in turn allows us to compute the electron numbers and magnetic moments as well as the energies of various ordered states.

The advantage of the real space recursion method over the conventional method in k-space are two folds: Firstly, it directly calculates the local densities of states and thus avoids the three dimensional integration over band dispersion within the Brillouin Zone; Secondly, all the proposed magnetically ordered states can be treated on equal footing within the supercell, the different states correspond to different sets of trial values of electron occupation numbers and thus it avoids using different geometries of Brillouin zone which can greatly reduce the systematic error during the numerical computation. Also, the computational time of real space recursion method increases linearly with the number of atoms in a primary cell while the k-space method increases quadratically with the number of atoms in a cell, thus, it has an advantage when a large number of atoms in the cell exist and many different magnetic states have to be taken into consideration for comparison.

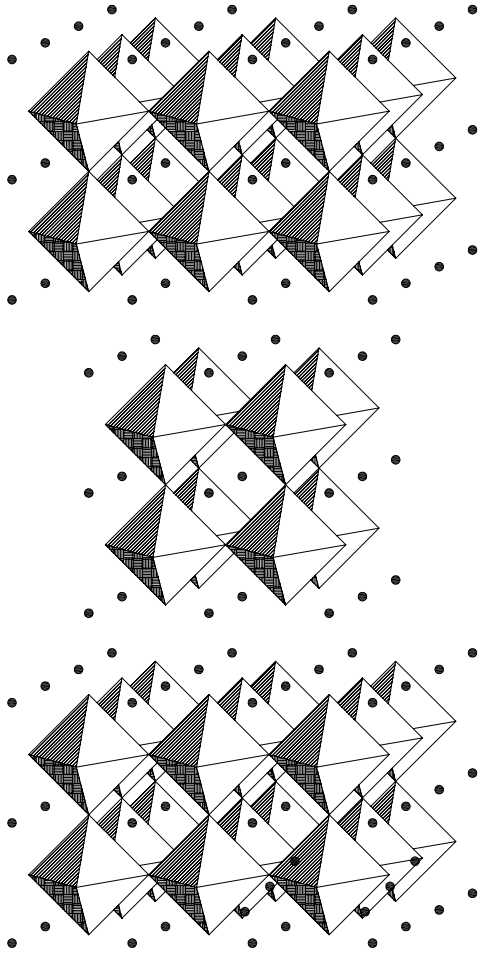

Fig. 1. Schematic view of the crystal structure of double-layered perovskite $Sr_2Y_{0.5}Ca_{0.5}Co_2O_7$.

3 Numerical results and discussion

The parameter set of the compound can be derived from the cluster model analysis of the photoemission spectra [5,6] as well as the ab initio local spin density approximation(LSDA) calculations [13,29]. The densities of states (DOS) of the end members $LaCoO_3$ and $SrCoO_3$ using these parameters are in an excellent agreement with both experiments and *ab initio* calculations [14]. The parameter set thus obtained is as follows: the bare on-site energies of Co-d and O-p orbitals are taken as $\varepsilon^0_d = -28$ eV and $\varepsilon_p = 0$ eV. The on-site Coulomb repulsion and Hund's coupling constants are set at $U = 5.0$ eV and $J_H = 0.84$ eV. The Slater-Koster parameters are estimated from those of $LaCoO_3$ using the well known scaling relations [30] $(ll'm) \propto d^{-2}$ for $l = l' = 1$ and $(ll'm) \propto d^{-3.5}$ for $l = 1, l' = 2$, where d is the bond length between two

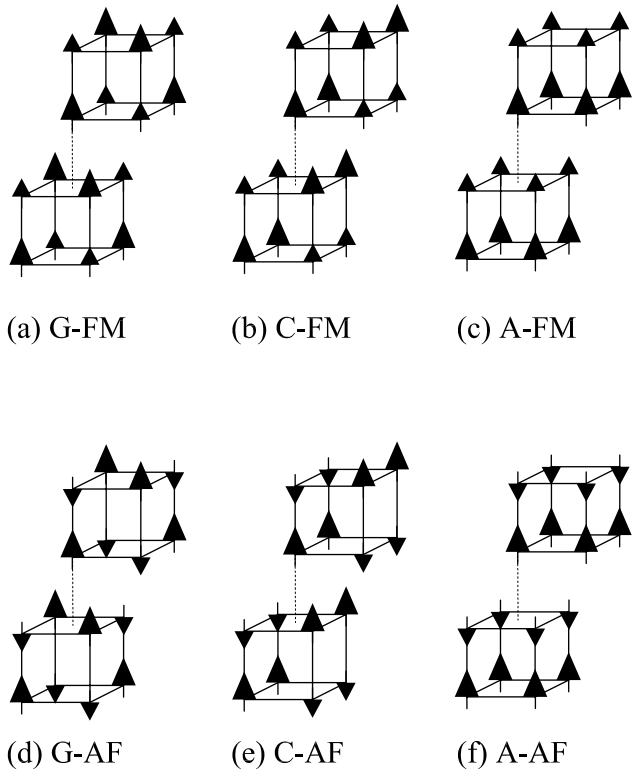

Fig. 2. Schematic diagram for various magnetic states. (a) G-FM state, (b) C-FM state, (c) A-FM state, (d) G-AF state, (e) C-AF state, and (f) A-AF state. The longer and shorter arrows represent the moments of different spin states of inequivalent cobalt ions.

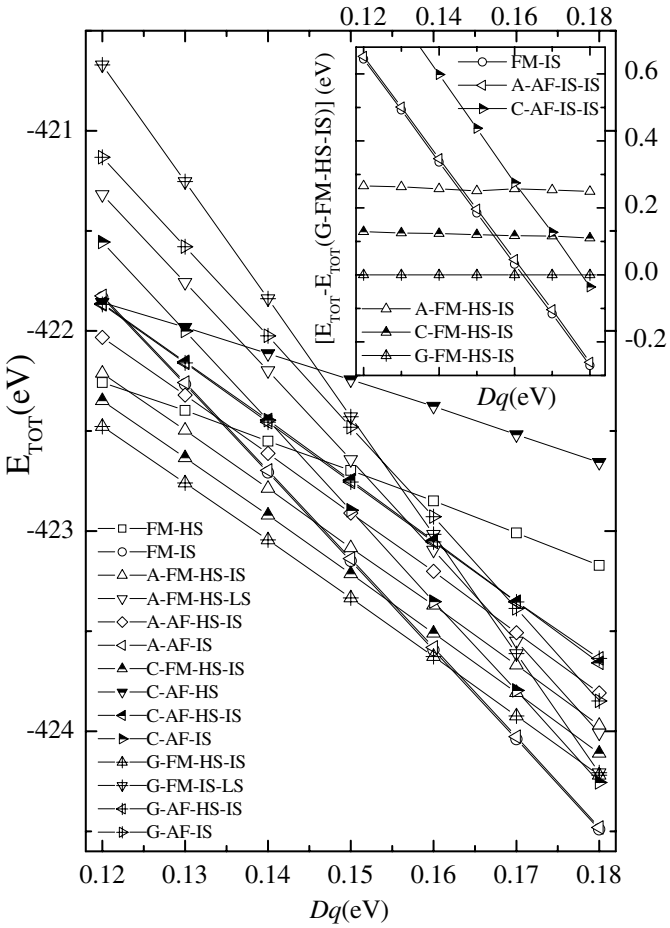

Fig. 3. The total energies (E_{TOT}) per double cell as a function of Dq. The inset is the relative energies ($E_{\triangle}$) with respect to that of the G-FM-HS-IS state. The other parameters are listed in the text.

atoms. The crystal structure of $Sr_2Y_{0.5}Ca_{0.5}Co_2O_7$ as shown in Figure 1 belongs to tetragonal crystal group and lattice constants are $a = 3.759$ Å and $c = 20.00$ Å [17], the Slater-Koster parameters of $LaCoO_3$ are $(pd\sigma) = -2.0$ eV, $(pd\pi) = 0.922$ eV, $(pp\sigma) = 0.6$ eV, and $(pp\pi) = -0.15$ eV, respectively [14]. The most probable magnetic ground state is searched as a function of electrostatic part of crystal-field-splitting Dq.

With the parameter set given above, we have investigated various magnetically ordered states of the compound shown in Figure 2, which include ferromagnetically ordered state(FM), nearest neighbor antiferromagnetically ordered state(G-AF), antiferromagnetically ordered chain along a-axis(C-AF), and the layer-type antiferromagnetically ordered state(A-AF). In addition, the ferromagnetically ordered state can be sub-divided into three ferromagnetic states denoted by the G-FM, C-FM, and A-FM whose neighboring spin states of Co ions are different and with a modulation vector similar to those antiferromagnetic states described above. In each magnetic state, three spin-states of Co ions are considered which amounts to 6 different spin configurations and $6 \times 6 - 6 = 30$ different magnetic states in total. The numerical studies show that some of these states are either not metastable or converge to other more stable states and some of these states are metastable but with much higher energy than other states. Therefore, we concentrate in the following those metastable states which are either the possible magnetic ground states or the low lying excited states of the compound.

In order to determine which spin structure is the most probable candidate for the ground state of $Sr_2Y_{0.5}Ca_{0.5}Co_2O_7$, we have calculated energies per double-cell of various magnetically ordered states as functions of Dq. The phase diagram is presented in Figure 3 for those low lying states, the horizontal axis denotes the electrostatic part of crystal field splitting and vertical axis represents the total energy of each state. To have a better view of those low lying states, the six lowest energy states are replotted in the inset of Figure 3. This figure shows that the ferromagnetically ordered states composed of nearest neighbor ordered high-spin and intermediate-spin states(G-FM-HS-IS) consistently have lower energy than other states when the crystal field splitting is small. While at large crystal field splitting, the ferromagnetically ordered state with uniform intermediate-spin (FM-IS) has the lowest energy and layer-type antiferromagnetically

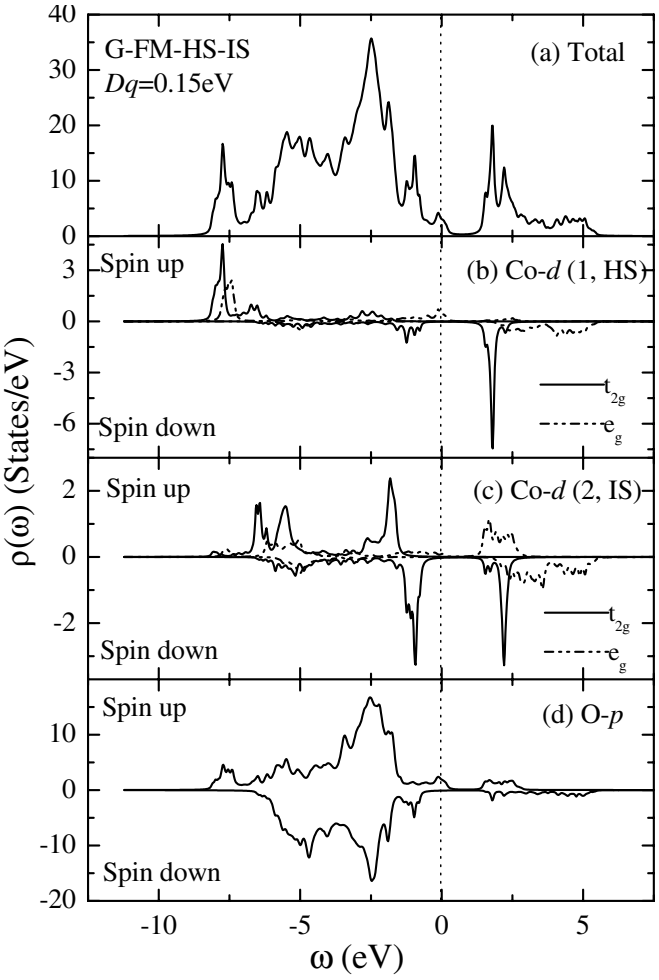

Fig. 4. The total density of states and partial densities of states for G-FM-HS-IS state. (a) TDOS, (b) PDOS for Co(1)-d orbitals, (c) PDOS for Co(2)-d orbitals, and (d) PDOS for all O-p orbitals. $Dq = 0.15$ eV and the other parameters are listed in the text.

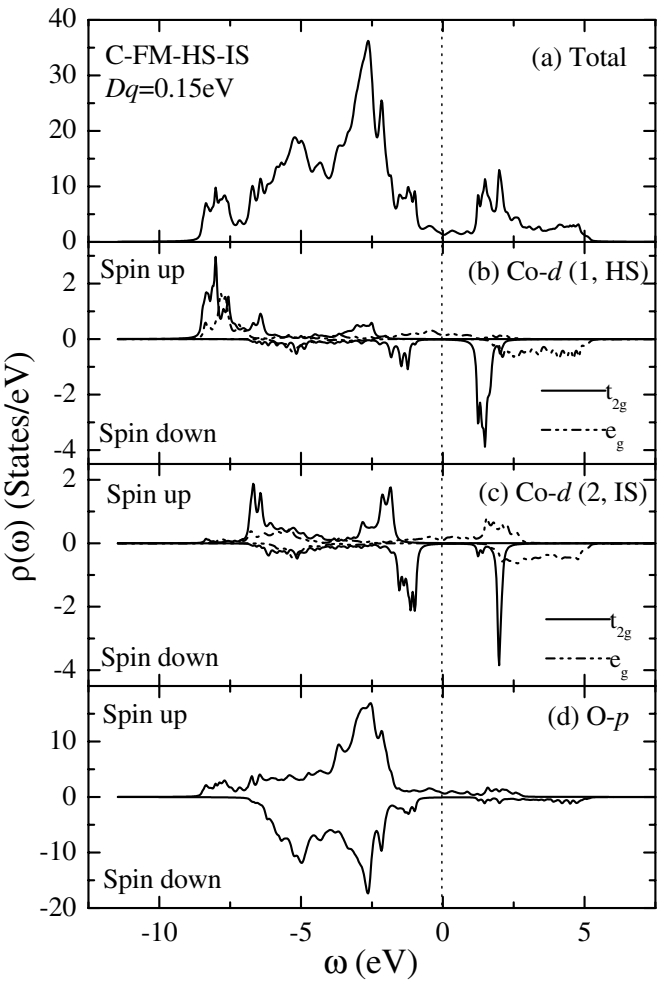

Fig. 5. The total density of states and partial densities of states for C-FM-HS-IS state. (a) TDOS, (b) PDOS for Co(1)-d orbitals, (c) PDOS for Co(2)-d orbitals, and (d) PDOS for all O-p orbitals. $Dq = 0.15$ eV and the other parameters are listed in the text.

ordered states with the intermediate-spin(A-AF-IS) serves as the first excited state. Although both G-FM-HS-IS state and FM-IS state are the possible magnetic ground states, only the G-FM-HS-IS state has the right average magnetic moment which is consistent with the experimental measurement. In the following, we concentrate mainly on the magnetic ground states and first excited states since they are the most relevant states to the properties measured in experiments.

The first state we consider is the high-spin(HS) and intermediate-spin(IS) nearest neighbor ordered ferromagnetic state(Fig. 2a, G-FM-HS-IS), which also happens to be the ground state in the range $Dq \leq 0.162$ eV. The total density of states (TDOS) and partial densities of states(PDOS) for Co(1,HS), Co(2,IS)-d orbitals and all oxygen-p orbitals are presented in Figure 4 for $Dq = 0.15$ eV, this state is a conductor since there exists finite density of states at Fermi energy($E_F \equiv 0$). The occupancies and magnetic moments of Co ions are 6.39 and $3.12\mu_B$ for Co(1,HS) site and 6.60 and $1.55\mu_B$ for Co(2,IS) site, respectively. The average effective magnetic moment is estimated to be $\mu_{eff} = \sqrt{0.5[\mu(1)(\mu(1)+2)+\mu(2)(\mu(2)+2)]} \approx 3.28\mu_B$ which is close to but higher than the experimentally measured value of $\mu_{eff} \approx 2.89\mu_B$ [17]. The analysis of the partial density of states reveals that the spectra weight below the Fermi energy are mainly contributed by the O-p orbitals except those satellite peaks near and deep below the Fermi energy. A close inspection of densities of states show that the Co-d's t_{2g} orbitals are quite localized while the e_g orbitals are rather extended and exhibit strong itinerancy. The DOS at the Fermi energy has mixed characters and are mainly contributed by the oxygen-p and HS Co-d orbitals. The electron occupancies of Co-d orbitals are larger than the value indicated by the ionic valence because of the strong covalency between Co-d and O-p orbitals.

The combination of HS and IS states seems to be a common feature for the magnetic ground state and low lying excited states when $Dq \leq 0.162$ eV. As can be seen in the phase diagram shown in Figure 3, the first and second excited states are also ferromagnetically ordered

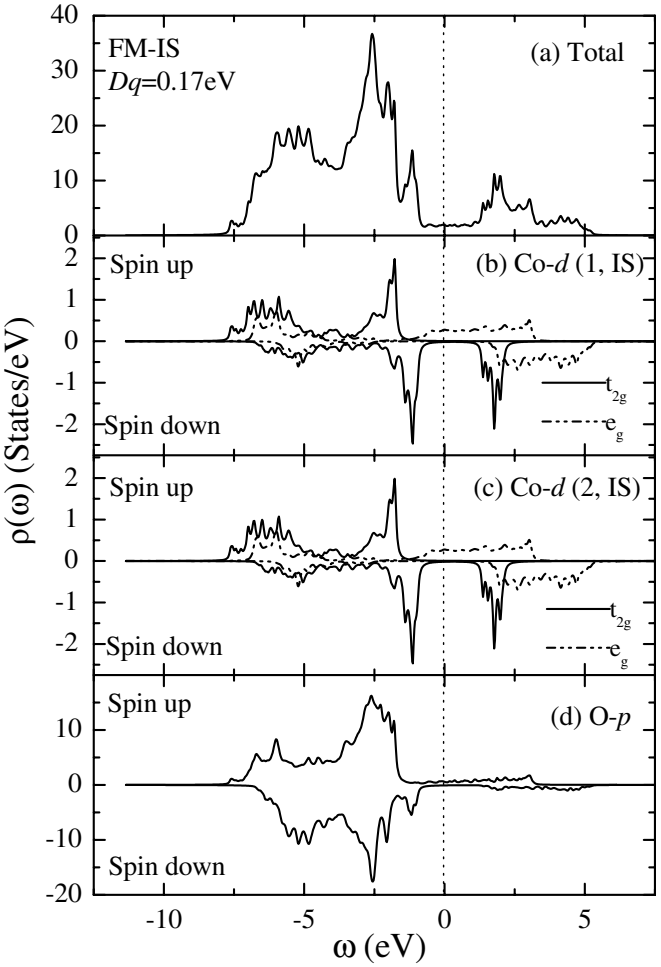

Fig. 6. The total density of states and partial densities of states for FM-IS state. (a) TDOS, (b) PDOS for Co(1)-*d* orbitals, (c) PDOS for Co(2)-*d* orbitals, and (d) PDOS for all O-*p* orbitals. $Dq = 0.17$ eV and the other parameters are listed in the text.

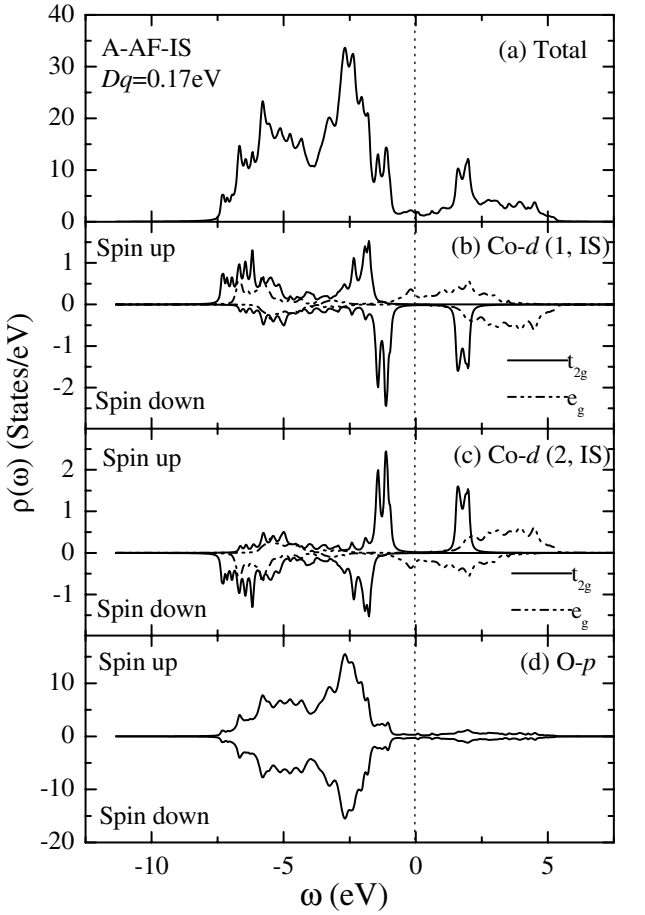

Fig. 7. The total density of states and partial densities of states for A-AF-IS state. (a) TDOS, (b) PDOS for Co(1)-*d* orbitals, (c) PDOS for Co(2)-*d* orbitals, and (d) PDOS for all O-*p* orbitals. $Dq = 0.17$ eV and the other parameters are listed in the text.

states composed of HS and IS states of Co ions, but with different modulation wave vectors. For example, the first excited state(C-FM-HS-IS) is the chain-type ferromagnetically ordered state(Fig. 2b) where the one dimensional ferromagnetically ordered HS chain and IS chain are organized into an neighboring alternating structure. The total density of states and partial densities of states shown in Figure 5 suggest that the overall feature of the density of states is similar to those of G-FM-HS-IS state although the DOS at Fermi energy is significantly reduced. The similarity arises because of the similar sizes of exchange field for the HS and IS Co-*d* orbitals in these two magnetic states. The peaks widths of Co-*d* related bands are somewhat enhanced due to the existence of one-dimensional chains which favors the itinerancy of *d*-electrons. The occupancies and magnetic moments of Co ions are 6.38 and $3.07\mu_B$ for Co(1,HS) site and 6.6 and $1.56\mu_B$ for Co(2,IS) site, respectively. The deduced effective magnetic moment is $\mu_{eff} \approx 3.25\mu_B$.

If the electrostatic crystal-field-splitting energy Dq is larger than 0.162 eV, the high-spin state is not favored and the magnetic ground state changes from the G-FM-HS-IS state into a uniform ferromagnetically ordered state composed of IS state(FM-IS). From the total as well as partial densities of states illustrated in Figure 6, one notices that the total band width is significantly reduced. This is so because the intermediate-spin state of Co ions has a smaller magnetic moment, the resulted exchange field is also much weaker than that of high-spin state of Co ions, thus the band splitting due to the exchange field is significantly reduced in comparison with that of mixed HS and IS ferromagnetically ordered state. The peaks in the density of states near the Fermi energy becomes more symmetrical because all the Co ions are in the same IS state. As before, this state also corresponds to a metallic state. The occupancy and magnetic moment of Co ions are 6.57 and $1.48\mu_B$. The corresponding effective magnetic moment is $\mu_{eff} \approx 2.27\mu_B$ which is much smaller than the measured value.

Unlike the situation in the low crystal field splitting $Dq \leq 0.162$ eV where both magnetic ground state and first excited state are ferromagnetic states and are separated

by a large energy difference, the first excited state for $Dq > 0.162$ eV is a layer-type antiferromagnetically ordered state composed of the same IS state of Co ions(A-AF-IS) and has a total energy in close proximity to the FM-IS ground state. As illustrated in Figure 7, the antiferromagnetic feature can be clearly distinguished in the PDOS of oxygen p-orbitals which are fully symmetrical due to the compensation of neighboring antiferromagnetically ordered layers. The PDOS of Co-d orbitals in neighboring planes also showed a mirror symmetry because of reversed magnetic moments. Because the magnetic moment in A-AF-IS state has a similar size as that of FM-IS state, the overall band width is also similar though the spin polarized DOS are dramatically different from each other. The occupancy and magnetic moment of Co ions are 6.58 and $1.48\mu_B$.

In addition to the 30 magnetic states studied above, we have, in fact, also investigated other magnetic states with different inter-double-layer magnetic coupling, but in the relevant Dq range to the studied material, only G-FM-HS-IS state and FM-IS state do have the lowest energy and correspond to the possible magnetic ground state. However, by further comparing with the experimentally measured effective magnetic moment, one finds that G-FM-HS-IS state is more closer to the experimental observation both in ferromagnetic ordering as well as in the size of magnetic moment while FM-IS state only has the right ferromagnetic ordering, but the size of magnetic moment is too small in comparing with the measured one. Thus, we conclude that the G-FM-HS-IS state is the best candidate for the experimentally observed magnetic state.

Another thing worth of mentioning is that although doped samples correspond to a metallic state in the band structure picture as demonstrated in the DOS shown in Figure 4, the presence of disorders, mixed phase, as well as grain boundary can easily induce electronic localization. Therefore, to have a better comparison between theoretical prediction and experimental measurement on transport property, single crystal samples are highly desirable.

4 Conclusion

In conclusion, various magnetic structures in an enlarged double cell of double layered perovskite $Sr_2Y_{0.5}Ca_{0.5}Co_2O_7$ are studied using the unrestricted Hartree-Fock approximation and the real-space recursion method, the phase diagram is obtained as functions of the electrostatic part of crystal-field splitting. In view of the measured effective magnetic moment, it is concluded that the G-FM-HS-IS state is the best candidate for the magnetic ground state of the system. The variable-range-hopping transport property of the compound is most probably resulted from the polycrystalline grain boundaries, disorders, and the mixed phase of $KClO_z$.

This work was supported in part by the National Basic Research Program of China (Grant Nos. 2007CB925104, 2004CB619003). We wish to acknowledge the partial financial support from the NNSFC under Grant No. 10474040, 10334090, 10523001, and "Excellent Youth Foundation"[10025419].

References

1. R.R. Heikes, R.C. Miller, R. Mazelsky, Physica **30**, 1600 (1964)
2. G.H. Jonker, J. Appl. Phys. **37**, 1424 (1966)
3. P.M. Raccah, J.B. Goodenough, J. Appl. Phys. **39**, 1209 (1967)
4. C.N.R. Rao, M. Seikh, C. Narayana, Topics in current chemistry **234**, 1 (2004)
5. J. Zaanen, G.A. Sawatzky, J. Solid State Chem. **88**, 8 (1990)
6. A. Chainani, M. Mathew, D.D. Sarma, Phys. Rev. B **46**, 9976 (1992)
7. L. Sudheendra, M. Seikh, A.R. Raju, C. Narayana, Chem. Phys. Lett. **340**, 275 (2001)
8. O. Toulemonde, N. N'Guyen, F. Studer, A. Traverse, J. Solid State Chem. **158**, 208 (2001)
9. S. Yamaguchi, H. Taniguchi, H. Takagi, T. Arima, Y. Tokura, J. Phys. Soc. Jpn. **54**, 1885 (1995)
10. G. Briceno, H. Chang, X. Sun, P. G. Schultz, X. D. Xiang, Science **270**, 273 (1995)
11. V. Golovanov, L. Mihaly, A. R. Moodenbaugh, Phys. Rev. B **53**, 8207 (1996)
12. S. Balamurugan, M. Xu, E. Takayama-Muromachi, J. Solid State Chem. **178**, 3431 (2005)
13. P. Ravindran, P. A. Korzhavyi, H. Fjellvag, A. Kjekshus, Phys. Rev. B **60**, 16423 (1999)
14. M. Zhuang, W.Y. Zhang, T. Zhou, N.B. Ming, Phys. Lett. A **255**, 354 (1999)
15. Y. Furukawa, S. Wada, Y. Yamada, J. Phys. Soc. Jpn **62**, 1127 (1993)
16. Y. Moritomo, K. Migashi, K. Matsuda, A. Nakamura, Phys. Rev. B **55**, 14725 (1997)
17. K. Yamaura, D.P. Young, R.J. Cava, Phys. Rev. B **63**, 064401(2001)
18. O.H. Hansteen, J. Solid State Chem. **141**, 212 (1998)
19. K. Takada, H. Sakurai, E. Takayama-Muromachi, F. Izumi, R.A. Dilanian, T. Sasaki, Nature (London) **422**, 53 (2003)
20. G. Baskaran, Phys. Rev. Lett. **91**, 97003 (2003)
21. R.E. Schaak, T. Klimczuk, M.L. Foo, R.J. Cava, Nature **424**, 527 (2003)
22. T. Mizokawa, A. Fujimori, Phys. Rev. B **54**, 5368 (1996)
23. S.V. Streltsov, A.S. Mylnikova, A.O. Shorikov, Z.V. Pchelkina, D.I. Khomskii, V.I. Anisimov, Phys. Rev. B **71**, 245114 (2005)
24. R.O. Kuzian, A.M. Dar, P. Sati, R. Hayn, Phys. Rev. B **74**, 155201 (2006)
25. J.C. Slater, G.F. Koster, Phys. Rev **94**, 1498 (1954)
26. Mark S. Hybertsen, E.B. Stechel, W. M. C. Foulkes, M. Schlter, Phys. Rev. B **45**, 10032 (1992)
27. V. Heine, R. Haydock, M.J. Kelly, in *Solid State Physics: Advances in Research and Applications*, edited by H. Ehrenreich, F. Seitz, D. Turnbull (Academic, New York, 1980), Vol. 35, p. 215.
28. R. Haydock, C.M.M. Nex, J. Phys. C **17**, 4783 (1984)
29. D.D. Sarma, N. Shanthi, S.R. Barman, N. Hamada, H. Sawada, K. Terakura, Phys. Rev. Lett. **75**, 1126 (1995)
30. W.A. Harrison, in *Electronic Structure and the Properties of Solids* (W.H. Freeman and Company, San Francisco, 1980)